NDT&E International 89 (2017) 74–80

Contents lists available at ScienceDirect

NDT&E International

journal homepage: www.elsevier.com/locate/ndteint

High temperature EMAT design for scanning or fixed point operation on magnetite coated steel

N. Lunn[a,*], S. Dixon[a], M.D.G. Potter[b]

[a] Department of Physics, University of Warwick, Coventry CV4 7AL, United Kingdom
[b] Sonemat Ltd., 34 High Street, Walsall, West Midlands WS9 8LZ, United Kingdom

ARTICLE INFO

Keywords:
EMAT
High temperature
Thickness measurement
Magnetostriction

ABSTRACT

Bulk thickness measurements were performed at elevated temperatures on magnetite coated low carbon steel pipe and aluminium samples, using a permanent magnet electromagnetic acoustic transducer (EMAT). The design presented here exploits the non-contact nature of EMATs to allow continuous operation at elevated temperatures without physical coupling, sample preparation (in the form of oxide scale removal), or active cooling of the EMAT. A non-linear change in signal amplitude was recorded as the magnetite coated sample was heated in a furnace, whereas a steady decrease in amplitude was observed in aluminium. For a magnetite coated pipe sample, after a dwell time of 3 h, a SNR of 33.4 dB was measured at 450 °C, whilst a SNR of 33.0 dB was found at 25 °C. No significant EMAT performance loss was observed after one month of continuous exposure to 450 °C. EMAT-sample lift-off performance was investigated at elevated temperature on magnetite coated steel; a single-shot SNR of 31 dB for 3.0 mm lift-off was recorded at 450 °C, highlighting the suitability of this design for scanning or continuous fixed point inspection at high temperature.

1. Introduction

A variety of industrial metal components operate continuously at elevated temperatures, including pipelines, boilers and reactors, over a range of industries, most notably power generation, petrochemical and metal processing. Performing in-service nondestructive evaluation (NDE) without the need for plant shutdown provides numerous advantages, such as reduced risk from thermal cycling and a decrease in the shutdown period and associated costs. Notwithstanding the wealth of research dedicated to inspection and condition monitoring at high temperature, there are continued efforts towards advancement of current high temperature NDE techniques [1,2].

High temperature piezoelectric transducers have been shown to operate without active cooling at up 750 °C [1]; their use has been reported for thickness measurements [3] and monitoring of cracks [4]. Piezoelectric transducers typically employ high temperature piezoelectric materials [5–9] or waveguides as thermal buffers [3,10] to provide continuous operation at elevated temperatures. Their main drawback is maintaining physical coupling to the specimen, requiring solid coupling [1], brazing [11] or direct deposition of a piezoelectric material [12]. Issues can arise in long term use of solid coupling techniques, such as thermally induced cycling stress from a thermal expansion mismatch between the transducer and sample. Industrial applications of high temperature transducers may require scanning techniques for inspection of large component areas, but high temperature piezoelectric transducers are currently limited to inspection at a permanently installed location. Therefore, a transducer capable of operating at a fixed point or in a scanning mode may prove beneficial for some applications.

Laser based methods are non-contact and able to operate on samples at elevated temperatures [13,14], although laser techniques are usually expensive and can be dependent on surface condition. Development of magnetostrictive patch transducers (MPTs) has been of interest for high temperature inspection, however these methods also require physical coupling of the transducer to the sample [15].

EMATs have been employed in thickness measurements and defect detection at high temperatures due to their noncontact nature, although this requires active cooling of a permanent magnet [16,17] or the use of a bulky electromagnet [18,19], limiting their use in some industrial settings. Laser-EMAT systems have also been employed successfully for high temperature operation [20–22], often with a water-cooled EMAT receiver, as EMATs generally provide greater efficiency in detection [23].

In this work, a robust and compact high temperature EMAT was developed, with a view to overcome some disadvantages of currently available high temperature ultrasound transducers. The design applies the advantages of EMATs to facilitate continuous operation at elevated temperatures without physical coupling, sample preparation (in the

* Corresponding author.

http://dx.doi.org/10.1016/j.ndteint.2017.04.001
Received 6 October 2016; Received in revised form 28 March 2017; Accepted 11 April 2017
Available online 13 April 2017

form of oxide scale removal), or active cooling, for use on oxide coated steel pipelines. The vast majority of industrial ferritic steel pipelines which operate continuously for long periods over 200 °C in a reducing atmosphere tend to develop a thin, well-adhered oxide surface coating (magnetite), which has been shown to greatly enhance EMAT efficiency [24,25]. This study exploits this increase in EMAT efficiency on magnetite coated steel to generate high signal-to-noise ratio (SNR) signals at temperatures up to 450 °C.

EMATs use a combination of static and dynamic magnetic fields to generate and detect ultrasound waves principally through two mechanisms, the Lorentz force and magnetostriction [26]; the mechanism that operates or dominates depends upon the EMAT design, and the electrical and magnetic properties of the sample. Lorentz force describes the EMAT generation and detection mechanism which operates on electrically conducting samples. When an AC current is driven through a coil, an eddy current is generated within the electromagnetic skin depth of the sample, this interacts with the static magnetic field to produce a Lorentz force on the free conducting electrons. Momentum exchange between the electrons and the lattice via collision generates ultrasound within the sample. EMATs can detect ultrasound through the reciprocal process.

Previous research has shown that the magnetostriction mechanism operates on magnetite coated steel [24,25], which can greatly enhance EMAT sensitivity depending on a number of factors, including strength of the static magnetic field, degree of bonding between the oxide coating and steel substrate, coating thickness and composition. Subject to these factors, the magnetostriction mechanism is able to generate signals in the region of two orders of magnitude greater on magnetite coated steel, when compared to bare steel samples. This variation is attributed to the fundamental difference between the generation and detection of ultrasound via magnetostriction when a highly magnetostrictive oxide coating is present, compared to the contribution from both the Lorentz force and magnetostriction on bare steel. Fundamentally, the Lorentz force mechanism produces a surface force acting on a conductive sample, whilst the magnetostrictive mechanism produces a shear body force across the entire magnetostrictive coating thickness on magnetite coated samples.

Magnetite exhibits magnetostriction, a reversible property of magnetic materials with magnetocrystalline anisotropy, resulting in a strain on exposure to a magnetic field, termed Joule magnetostriction; the reverse is the Villari effect [27]. An alternating current applied through the coil generates a dynamic magnetic field, resulting in oscillating magnetostrictive strains within the coating which launch ultrasound waves into the bulk of the steel [28]. Magnetostriction is highly nonlinear with change in the applied magnetic field, whereas the Lorentz force exhibits a linear relationship [29,30].

This paper presents a bulk shear wave EMAT design for pulse echo thickness measurements on industrial magnetite coated steel pipe and aluminium samples at temperatures up to 450 °C. The EMAT lift-off performance was investigated to evaluate the suitability for scanning inspections at high temperature.

2. High temperature EMAT

A radially polarized bulk shear wave EMAT (Sonemat, HWS2035-VC) was used, containing a spiral coil and a permanent magnet. A cross-sectional diagram of the high temperature EMAT design is shown in Fig. 1. The magnet is a high strength, high Curie point permanent magnet grade, that resists permanent demagnetization at higher temperatures; although it exhibits a lower magnetic flux density when heated. A static magnetic field, directed into the sample, is provided by a cubic magnet 25 mm in length, with a magnetic flux density of roughly 0.36 T at the surface of the magnet at ambient temperature. Similar to previous work [19], a hand wound spiral coil was encapsulated between two 0.5 mm thick alumina ceramic discs using 0.2 mm diameter bare copper wire; the front ceramic disc acts as a wear plate to protect the coil. The coil had 20 turns with a 0.2 mm spacing for the alumina ceramic adhesive, which functioned as electrical insulation. A 0.1 mm thick copper foil was placed between the magnet and coil, providing electromagnetic shielding [31] to reduce ultrasound generation within the magnet. The EMAT was housed in a stainless steel casing to provide electromagnetic and capacitive shielding of the EMAT, and to provide protection during measurements. To withstand elevated temperatures, a coaxial cable with ceramic as the inner insulator was used for connecting the EMAT to the pulser-receiver electronics.

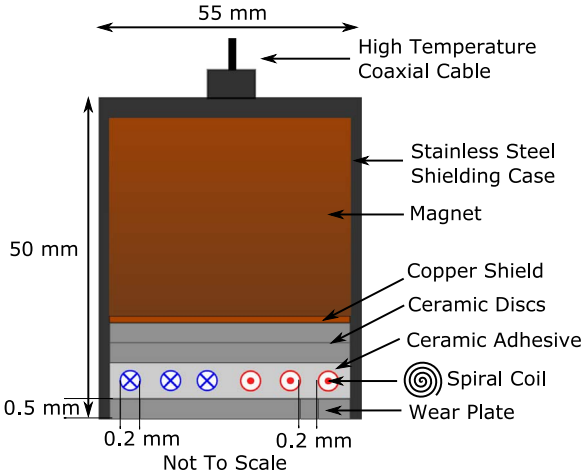

Fig. 1. Schematic cross-sectional view of the high temperature EMAT.

3. Experimental method

3.1. Experimental setup on magnetite coated steel

Two industrial magnetite coated low carbon steel pipe samples were used, termed sample A and B. The magnetite thickness was between 0.1 and 0.2 mm; this variation arises from the nature of growth of high temperature oxide scales in an industrial environment, where growth conditions can change due to a number factors, such as localized surface condition, temperature and composition. Average magnetite coating thickness was determined using a micrometer at a number of positions with and without the coating. Sample A had a stepped inner diameter, the maximum step at 6.8 mm and minimum step at 2.6 mm; both of these steps were tested to evaluate change in EMAT performance with sample thickness. Sample B had a uniform thickness of 6.8 mm. Both samples A and B had an outer pipe diameter of 150 mm.

The experimental setup of the pulse-echo bulk thickness measurement is illustrated in Fig. 2. A pulser-receiver unit (Sonemat, PR 5000) was used to provide a spike driving current pulse, at 450 V with a 100 ns pulse width, to excite the coil in generation, and wideband low-noise signal amplification in detection. A variable transformer was used, which allows one to change the voltage supply to the pulser-receiver, varying it from the mains supply voltage at ≈240 V. For example, with a variable setting at 100% the maximum driving current pulse was 28 A, whilst at 10% the maximum driving current pulse was

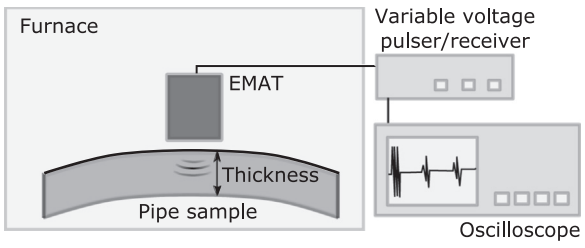

Fig. 2. Experimental set-up used to assess EMAT performance at high temperature.

5 A, this was determined by recording the voltage across a 0.1 Ω resistor in the discharge current path as the EMAT coil was pulsed. The variation of the driving current amplitude ensures the amplifier is within a linear range during detection; large signals generated using magnetite are able to saturate the amplifier and this should be avoided for quantitative measurements. For direct evaluation and comparison of the same sample under different conditions, an identical current pulse setting was used. The results were recorded using a digital oscilloscope (Tektronix, DPO2014) for single shot data, and averaged data (32×) to improve signal to noise ratio (SNR).

3.2. Experimental setup on aluminium

A 10 mm thick aluminium sample was used to compare results with the magnetite coated steel samples, as the signal in aluminium is solely due to the Lorentz force mechanism. Greatly decreased signal amplitudes were generated on aluminium compared to the magnetite coated samples, when using the Sonemat PR5000 pulser-receiver system with the same EMAT drive current; this difference is due to the relatively large signals generated via the magnetostriction mechanism on these magnetite coated steel samples, compared to the Lorenz force mechanism on aluminium, such that a direct comparison with identical hardware and drive current is not possible. Thus, to produce the most suitable signal on aluminium an alternative pulser-receiver system was used. A conventional flaw detector (Sonatest, Masterscan D-70) was used as the pulser-receiver with a drive voltage of 450 V and 100 ns pulse width, along with an EMAT averaging adapter (Sonemat, GS2020), which provides increased signal-to-noise performance via a 128 point running average and automatic gain control (AGC). This set-up produced a maximum driving current pulse of 12 A.

3.3. Performance with temperature

A furnace (Pyro Therm Furnaces, ITEMP 14/15) was used to heat the sample, EMAT and cable to the required temperature for a dwell time of 3 h before data acquisition. The temperature at the sample surface was recorded using a K-type thermocouple clamped to the sample. On heating the furnace temperature read lower than the sample surface temperature. The temperature difference was attributed to a thermal gradient established within the furnace, where the lower furnace regions are warmer due to the position of the heating elements. The furnace thermocouple is fixed at the top of the furnace, whereas the sample was placed at the base of the furnace. Table 1 shows the furnace and sample surface temperatures recorded for the 6.8 mm step on sample A. The sample and EMAT bulk temperatures were between these values, depending on thermal diffusivity, dwell time and furnace position.

3.4. Long term performance

The EMAT was held in a furnace for one month to investigate the high temperature performance over a longer period of time. A measurement was recorded on a 12 mm magnetite coated low carbon steel sample, termed Sample C, at 450 °C before and after one month of continuous exposure of the EMAT to 450 °C. The sample was not heated during this time in order to minimize changes in the magnetite coating thickness, as long term exposure to 450 °C may have caused favourable magnetite growth conditions; this had the potential to cause signal variation not attributed to changes in long term EMAT performance.

Table 1
Furnace and sample surface temperatures.

Furnace temperature (°C)	Sample surface temperature (°C)
25	26
50	55
150	171
250	278
350	378
425	458

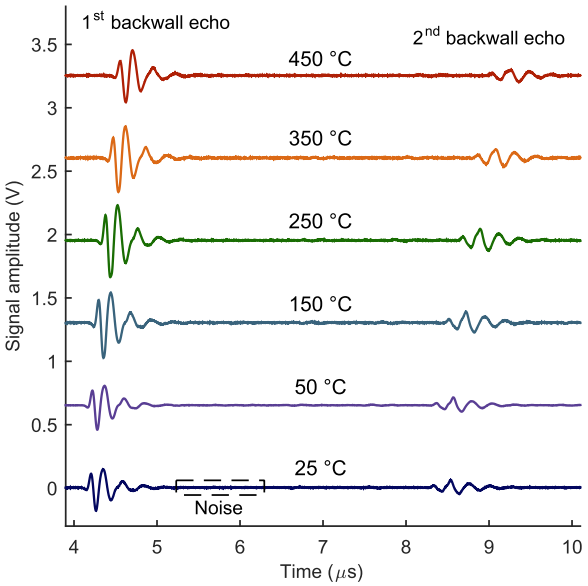

Fig. 3. Signal amplitude on 6.8 mm thick sample A at temperatures between 25 °C and 450 °C, showing the first and second backwall echoes.

3.5. Performance with lift-off

Lift-off measurements were made at 450 °C for 2.0 mm, 2.5 mm and 3.0 mm lift-off on sample B; lift-off was provided by a stack of 0.5 mm thick alumina ceramic discs.

4. Results and discussion

4.1. Performance with temperature on magnetite coated steel

The pulse-echo signal amplitude for the first and second backwall echoes at range of temperatures from 25 °C to 450 °C on the 6.8 mm step of sample A are shown in Fig. 3. The peak-to-peak voltage and SNR of the first echo against temperature for the 6.8 mm step on sample A are displayed in Figs. 4 and 5, respectively. The y-axis lower limit in Figs. 4 and 5 is set to zero to emphasize the appreciable change in peak-to-peak voltage and relatively small change in SNR between 25 °C and 450 °C, as these differences are substantial considering the increased noise recorded at higher temperatures. SNR was calculated

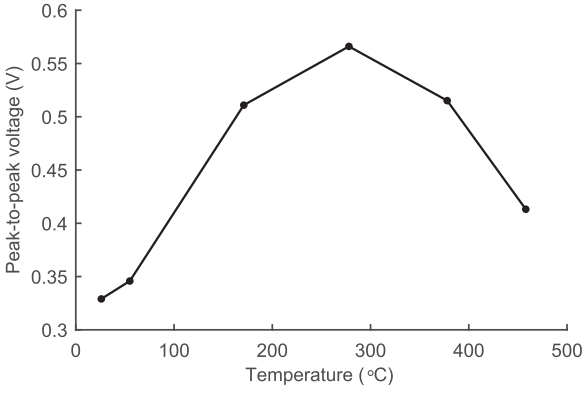

Fig. 4. First backwall echo peak-to-peak signal voltage on 6.8 mm thick sample A at temperatures between 25 °C and 450 °C.

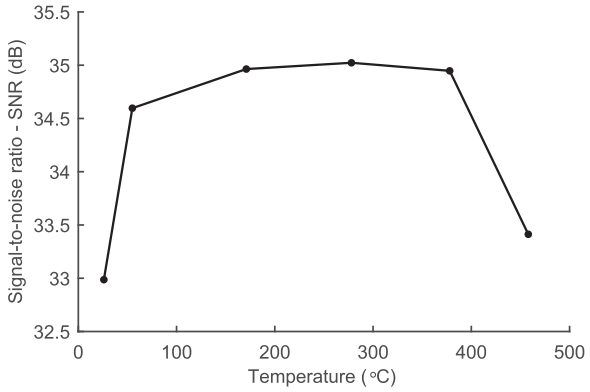

Fig. 5. First backwall echo SNR on 6.8 mm thick sample A at temperatures between 25 °C and 450 °C.

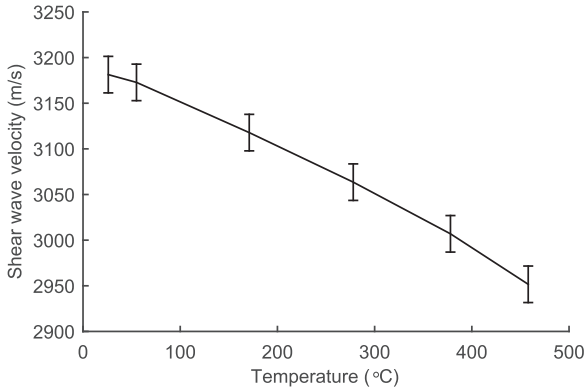

Fig. 6. Shear wave velocity at temperatures between 25 °C and 450 °C on sample A, including a thickness correction for thermal expansion.

using Eq. (1), where SNR_{dB} is the signal-to-noise-ratio in decibels, A_{signal} is the maximum signal amplitude within the echo and A_{noise} is the average value of a number of noise peaks for a region of noise after the echo. The region of noise used to calculate SNRs is identified on the figures for reference.

$$SNR_{dB} = 20\log_{10}\left(\frac{A_{signal}}{A_{noise}}\right) \tag{1}$$

The backwall echoes are clearly identifiable from room temperature up to 450 °C. It is evident that there is a non-linear change in signal amplitude with increasing temperature, with a maximum signal amplitude at approximately 300 °C. Most importantly for high temperature measurements, there is a greater signal amplitude of 0.41 V with 33.4 dB SNR at 450 °C, when compared to 0.33 V with 33.0 dB SNR at 25 °C.

This non-linear behaviour could be attributed to the dominance of the magnetostrictive mechanism, where magnetostrictive strain coefficients [29] and ultrasound signal amplitude vary non-linearly with change in the applied magnetic field; this relies on the assumption that the field strength of the EMAT magnet decreases with increasing temperature, given that magnetic flux density measurement at elevated temperatures was not measured. This follows from previous research [25] showing the non-linear change in signal amplitude with change in EMAT static magnetic field, for magnetite coated steel pipes, where a maximum signal amplitude was observed at lower magnetic fields of ≈0.35 T at room temperature.

Recent literature on modelling and experimental validation of EMAT magnetostrictive behaviour has focused on the magnetostriction contribution on bare steels [30,32], found to be between 5% and 10% depending on steel grade, where the Lorentz force is dominant. To the best of the authors' knowledge, a comprehensive study of high temperature operation of EMATs on magnetite coated steels, where magnetostriction is the dominant mechanism, has not been reported in the literature. This is most likely due to the complex non-linear nature of the magnetostrictive mechanism on such materials, and the number of dependent variables.

The change in shear wave velocity and shear wave signal attenuation with temperature for the 6.8 mm step on sample A are plotted in Figs. 6 and 7, respectively; the values were calculated in the time domain. A thickness correction for thermal expansion was applied using Eq. (2) [19], where d is sample thickness at temperature T, d_0 is the sample thickness at T_0=25 °C and α(T) is the thermal expansion coefficient of steel at temperature T. The time of flight difference, Δt, between the first and second echoes was calculated by finding the difference between the time point of maximum signal amplitude of both echoes. The errors originate from determination of the sample thickness and time of flight between successive backwall echoes. The shear wave velocity was calculated from Eq. (3). The shear wave signal

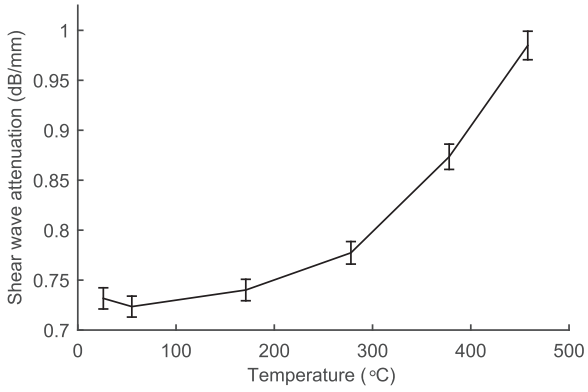

Fig. 7. Shear wave signal attenuation at temperatures between 25 °C and 450 °C on sample A, including a thickness correction for thermal expansion.

attenuation obtained directly from the time domain waveform was calculated using Eq. (4), where A_1 and A_2 represent the maximum signal amplitude of the first and second echoes, respectively, however diffraction effects were neglected.

$$d = d_0[1 + \alpha(T)(T - T_0)] \tag{2}$$

$$v = \frac{2d}{\Delta t} \tag{3}$$

$$\alpha = \frac{1}{2d}20\log_{10}\left(\frac{A_1}{A_2}\right) \tag{4}$$

The shear wave velocity displays a steady decrease with increasing temperature, observed from the increase in echo arrival time, from 3180 m/s at 25 °C to 2950 m/s at 450 °C; the velocity increase is primarily as a result of change in the elastic constants with increasing temperature. The shear velocity values calculated are similar to those reported in literature for low carbon steel [13,33]. The change in velocity with temperature is an import consideration for thickness measurement calibration, as if not taken into account errors will occur during inspection.

The shear wave signal attenuation undergoes an increase at elevated temperatures, from 0.73 dB/mm at 25 °C to 0.98 dB/mm at 450 °C. In general ultrasound attenuation within a sample is the result of a various mechanisms, including absorption, scattering and diffraction effects. Over this temperature range, increased attenuation is attributed to greater scattering from increased thermal phonon-phonon interactions, rather than change in the microstructure [34]. Despite the increase in attenuation, both the first and second echo signal amplitude at 450 °C are adequate for thickness measurements.

The frequency content of the signals was examined via a fast Fourier transform (FFT) to a windowed section of a backwall echo. The

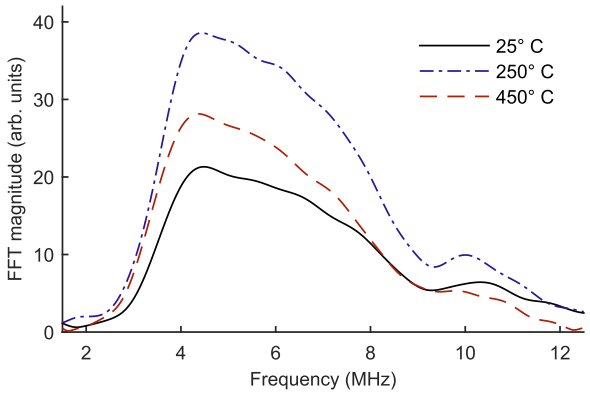

Fig. 8. Magnitude FFT of a windowed section of the first backwall echo on 6.8 mm thick sample A for 25 °C, 250 °C and 450 °C.

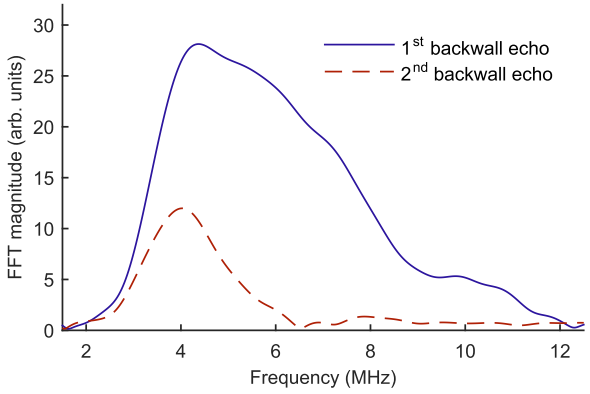

Fig. 9. Magnitude FFT of a windowed section of the first and second backwall echoes on 6.8 mm thick sample A at 450 °C.

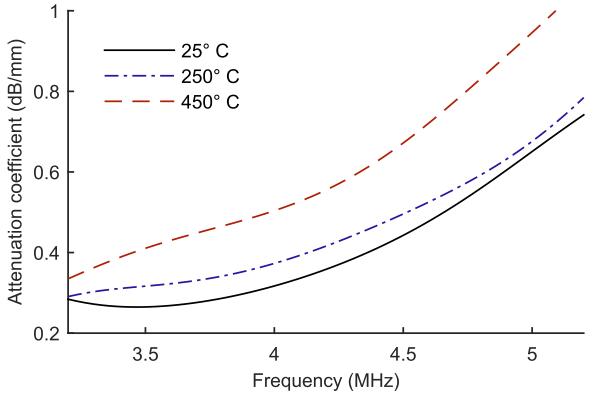

Fig. 10. Frequency dependent attenuation coefficient of sample A at 25 °C, 250 °C and 450 °C.

first backwall echo frequency content is shown in Fig. 8 at 25 °C, 250 °C and 450 °C. The first and second back-wall echo frequency content at 450 °C are displayed in Fig. 9. The signal is relatively broadband, with a maximum magnitude at a frequency of ≈4.5 MHz. A significant reduction in the higher frequency content of the second back-wall echo is observed, likely due to greater attenuation of higher frequencies which is more distinct with increasing temperature. This is highlighted by the frequency dependent attenuation coefficient, calculated using Eq. (4), where A_1 and A_2 represent the FFT magnitude of the first and second backwall echoes, respectively; these results are displayed in Fig. 10 at 25 °C, 250 °C, and 450 °C.

Signal amplitudes on the minimum step of sample A, with a thickness of 2.6 mm, are presented in Fig. 11 for 25 °C and 450 °C. The initial excitation noise from the driving pulse is included to

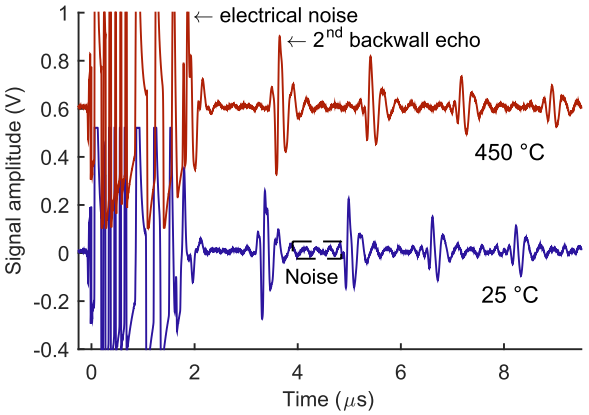

Fig. 11. Signal amplitude on 2.6 mm thick sample A at 25 °C and 450 °C, showing the initial electrical noise and series of reverberations.

indicate the loss of the first backwall echo within the noise, such that the second to fifth backwall echoes are displayed. The excitation noise with a dead time of ≈2 μs is longer than usual for this type of spiral EMAT coil, most likely due to the rigid encapsulation of the coil within the ceramic adhesive. For the second backwall echo the peak-to-peak voltage at 450 °C is 0.56 V with a SNR of 35.8 dB, while at 25 °C a lower peak-to-peak voltage of 0.53 V at SNR 32.9 dB was measured; despite the loss of the first backwall echo, subsequent echoes can be resolved in the time domain and their signal amplitudes are more than adequate for thickness measurements in this case.

4.2. Performance with temperature on aluminium

The pulse-echo signal amplitude for the first and second backwall echoes at range of temperatures from 25 °C to 450 °C on the 10 mm aluminium sample are shown in Fig. 12. The peak-to-peak voltage and SNR of the first echo against temperature for the 6.8 mm step on sample A are displayed in Figs. 13 and 14. The first backwall echoes in aluminium are distinguishable from room temperature up to 350 °C, whereas the first backwall echo at 450 °C is not clearly defined. The results show a steady decrease in signal amplitude with increasing temperature in aluminium, with a peak-to-peak voltage of 24 V with 18.3 dB at 25 °C and 0.05 V with 4.9 dB at 450 °C.

As the Lorentz force is the sole generation and detection mechan-

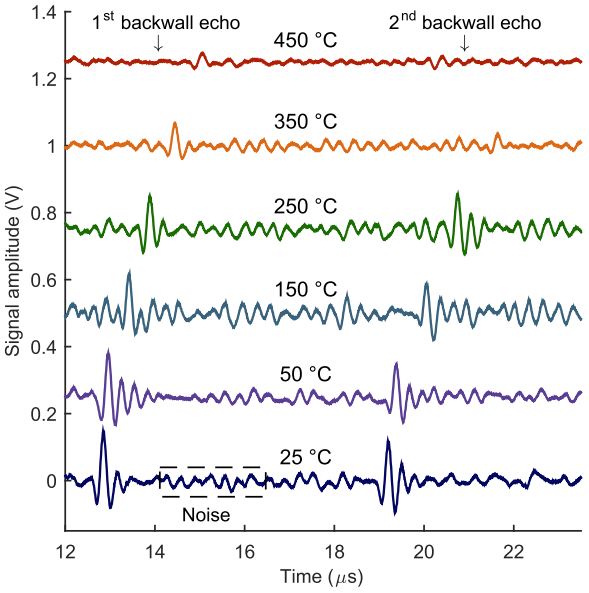

Fig. 12. Signal amplitude on 10 mm thick aluminium sample at temperatures between 25 °C and 450 °C, showing the first and second backwall echoes.

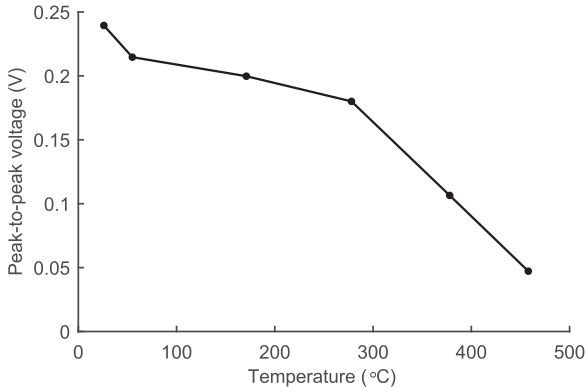

Fig. 13. First backwall echo peak-to-peak signal voltage on 10 mm thick aluminium sample at temperatures between 25 °C and 450 °C.

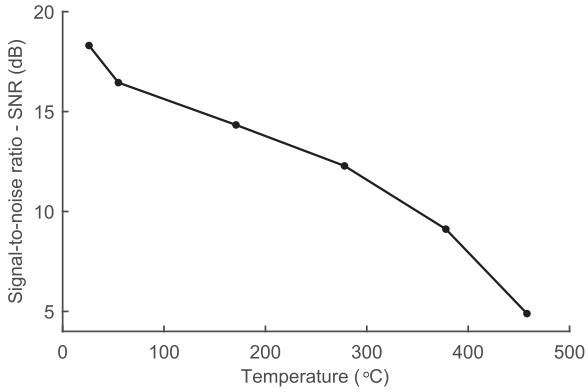

Fig. 14. First backwall echo SNR on 10 mm thick aluminium sample at temperatures between 25 °C and 450 °C.

ism when EMATs operate on aluminium, we can contribute a proportion of the loss in signal amplitude at elevated temperatures temperature to a decrease in the Lorentz force, in addition to increased ultrasound attenuation. In pulse-echo mode, the Lorentz force is proportional to the square of magnetic field, which is dominated by the static magnetic field at the coil driving currents used in this study. Hence, the Lorentz force most likely decreases from a reduction in the EMAT magnet field strength at elevated temperatures. Therefore, it can be estimated that the non-linear change in signal amplitude with increasing temperature observed on magnetite coated steel samples is due to the dominance of the magnetostriction mechanism.

4.3. Long term performance

The long term performance was investigated by subjecting the EMAT to 450 °C continuously for one month; the first four backwall echoes before and after one month are displayed in Fig. 15 for sample C. The first backwall echo SNR before heating was 35.8 dB, and the first backwall echo SNR was 35.7 dB after one month. Effort was made to place the EMAT on the same sample position for measurements before and after heating, however, the positioning may not have been identical; this could have led to a difference in the signal amplitude due to difference in properties of the magnetite coating, such as thickness and composition. Yet, no significant loss in performance was observed, indicating the potential application of this high temperature EMAT design for continuous inspection at elevated temperatures.

4.4. Performance with lift-off

The EMAT lift-off performance at 450 °C was evaluated on sample B at 2.0 mm, 2.5 mm and 3.0 mm lift-off between the sample and

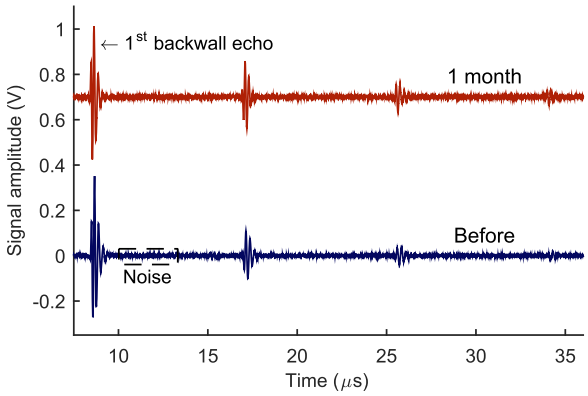

Fig. 15. Signal amplitude on sample C at 450 °C before and after one month of continuous exposure of the EMAT to 450 °C, showing the first four backwall echoes.

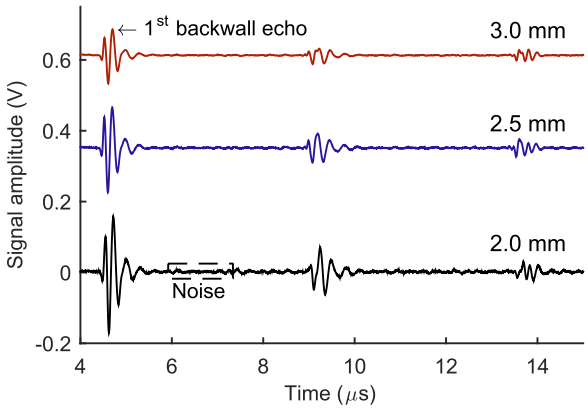

Fig. 16. Signal amplitude on sample B at 450 °C with EMAT lift-off at 2.0 mm, 2.5 mm and 3.0 mm, showing the first three backwall echoes. Acoustic birefringence [36] can be identified, due to peak splitting of the second and third backwall echoes.

EMAT. The first three back-wall echoes are shown for each of these lift-off values in Fig. 16. The SNR calculated for the first back-wall echo at each lift-off is 35.8 dB, 33.8 dB and 31.0 dB for 2.0 mm, 2.5 mm and 3.0 mm, respectively. As expected, there is a decrease in signal amplitude and SNR with increasing lift-off; it is reported widely in the literature that signal amplitude decreases exponentially with increasing lift-off for EMATs [35], with lift-off values of around 1 mm exhibiting a significant effect on SNR. Although the first backwall echo SNR exhibits a decrease from 35.8 dB at 2 mm to 31.0 dB at 3 mm, these signals are adequate for thickness measurements at 450 °C at all the lift-off values tested. This demonstrates the applicability of this EMAT for high temperature scanning inspections of magnetite coated low carbon steel pipelines without shutdown.

5. Conclusion

Progress has been made towards design and performance evaluation of a high temperature permanent magnet EMAT, capable of continuous operation up to 450 °C without cooling on magnetite coated low carbon steel; such oxide coatings are typical of mild steel components operating at elevated temperatures. Measurements conducted on an industrial magnetite coated sample have shown an increase in the single-shot SNR of 33.4 dB at 450 °C, when compared to 33.0 dB at 25 °C. The change in signal amplitude at elevated temperature could be due to the non-linear relationship between signal amplitude and the applied magnetic field for the EMAT magnetostriction mechanism, which tends to dominate when using EMATs on magnetite coated samples, depending on a number of factors. The high temperature EMAT performance on aluminium, on which ultrasound is generated and detected solely via the Lorentz force mechanism, was

observed to decrease with increasing temperature up to 450 °C, where the first backwall echo is not clearly defined from the noise level. Future work is required to comprehensively establish a model with experimental validation of this non-linear behaviour on magnetite coated samples.

There was found to be no significant performance loss with continuous exposure of the EMAT to 450 °C for one month; this suggests the suitability of this high temperature EMAT for continuous inspection at elevated temperatures without cooling. The applicability of this EMAT for scanning inspections at high temperature was also highlighted, where single-shot SNR of 31.0 dB was measured at 450 °C with a 3 mm lift-off. The high temperature cabling developed for the EMAT was capable of surviving at elevated temperatures, as was every other component used in the EMAT construction.

Acknowledgements

The authors would like to acknowledge funding and support for this research provided by EPSRC grant EP/I017704/1 for the Centre for Doctoral Training in NDE and project sponsor Sonemat Ltd. Details of the underlying data in support of this article can be accessed here: http://www2.warwick.ac.uk/fac/sci/physics/research/ultra/research/NDTE_NL1.zip.

References

[1] Atkinson I, Gregory C, Kelly SP, Kirk KJ. Ultrasmart: Developments in ultrasonic flaw detection and monitoring for high temperature plant applications. In: ASME 2007 Pressure Vessels and Piping Conference, American Society of Mechanical Engineers; 2007. p. 573–85.
[2] Budimir M, Mohimi A, Selcuk C, Gan T-H. High temperature nde ultrasound transducers for condition monitoring of superheated steam pipes in nuclear power plants. In: Proceedings of the International Conference Nuclear Energy for New Europe, Bovec, Slovenia; 2011.
[3] Cegla FB, Cawley P, Allin J, Davies J. High-temperature (>500 °C) wall thickness monitoring using dry-coupled ultrasonic waveguide transducers. IEEE Trans Ultrason, Ferroelectr, Freq Control 2011;58(1):156–67.
[4] Cegla F, Jarvis A, Davies J. High temperature ultrasonic crack monitoring using sh waves. NDT & E Int 2011;44(8):669–79.
[5] Kažys R, Voleišis A, Voleišienė B. High temperature ultrasonic transducers: review. Ultragarsas (Ultrasound) 2008;63(2):7–17.
[6] Zhang S, Yu F. Piezoelectric materials for high temperature sensors. J Am Ceram Soc 2011;94(10):3153–70.
[7] Jiang X, Kim K, Zhang S, Johnson J, Salazar G. High-temperature piezoelectric sensing. Sensors 2013;14(1):144–69.
[8] Hou R, Hutson D, Kirk KJ. Development of sputtered ALN thin-film ultrasonic transducers for durable high-temperature applications. Insight-Non-Destr Test Cond Monit 2013;55(6):302–7.
[9] Amini MH, Sinclair AN, Coyle TW. A new high-temperature ultrasonic transducer for continuous inspection. IEEE Trans Ultrason, Ferroelectr, Freq Control 2016;63(3):448–55.
[10] Jen C-K, Cao B, Nguyen KT, Loong CA, Legoux J-G. On-line ultrasonic monitoring of a die-casting process using buffer rods. Ultrasonics 1997;35(5):335–44.
[11] Shih JL, Kobayashi M, Jen CK. Flexible metallic ultrasonic transducers for structural health monitoring of pipes at high temperatures. IEEE Trans Ultrason, Ferroelectr, Freq Control 2010;57(9):2103–10.
[12] Burrows SE, McAughey KL, Edwards RS, Dixon S. Sol–gel prepared bismuth titanate for high temperature ultrasound transducers. RSC Adv 2012;2(9):3678–83.
[13] Scruby C, Moss B. Non-contact ultrasonic measurements on steel at elevated temperatures. NDT & E Int 1993;26(4):177–88.
[14] Nakano H, Nagai S. Crack measurements by laser ultrasonic at high temperatures. Jpn J Appl Phys 1993;32(5S):2540.
[15] Heo T, Cho SH, Thin-plate-type embedded ultrasonic transducer based on magnetostriction for the thickness monitoring of the secondary piping system of a nuclear power plant. Nucl Eng Technol.
[16] Dixon S, Edwards C, Reed J, Palmer SB. Using EMATs to measure the wall thickness of hot galvanizing kettles. Insight 1995;37(5):368–70.
[17] Kogia M, Gan TH, Balachandran W, Livadas M, Kappatos V, Szabo I, Mohimi A, Round A. High temperature shear horizontal electromagnetic acoustic transducer for guided wave inspection. Sensors 2016;16(4):582.
[18] Hernandez-Valle F, Dixon S. Initial tests for designing a high temperature emat with pulsed electromagnet. NDT & E Int 2010;43(2):171–5.
[19] Hernandez-Valle F, Dixon S. Pulsed electromagnet emat for ultrasonic measurements at elevated temperatures. Insight-Non-Destr Test Cond Monit 2011;53(2):96–9.
[20] Idris A, Edwards C, Palmer S. Acoustic wave measurements at elevated temperature using a pulsed laser generator and an electromagnetic acoustic transducer detector. Nondestruct Test Eval 1994;11(4):195–213.
[21] Baillie I, Griffith P, Jian X, Dixon S. Implementing an ultrasonic inspection system to find surface and internal defects in hot, moving steel using emats. Insight-Non-Destr Test Cond Monit 2007;49(2):87–92.
[22] Burrows SE, Fan Y, Dixon S. High temperature thickness measurements of stainless steel and low carbon steel using electromagnetic acoustic transducers. NDT & E Int 2014;68:73–7.
[23] Murfin A, Soden R, Hatrick D, Dewhurst RJ. Laser-ultrasound detection systems: a comparative study with rayleigh waves. Meas Sci Technol 2000;11(8):1208.
[24] Gori M, Giamboni S, d'Alessio E, Ghia S, Cernuschi F. EMAT transducers and thickness characterization on aged boiler tubes. Ultrasonics 1996;34(2):339–42.
[25] Dixon S, Edwards C, Palmer S, Crowther P. Electromagnetic acoustic transducers for testing power station boiler tubes. In: Review of progress in quantitative nondestructive evaluation, Springer; 1999. p. 1995–2000.
[26] Hirao M, Ogi H. EMATs for science and industry: noncontacting ultrasonic measurements. Boston: Kluwer Academic Publishers; 2003.
[27] Kittel C. Introduction to solid state physics. Hoboken: J. Whiley & Sons, Inc.; 2005.
[28] Kim YY, Kwon YE. Review of magnetostrictive patch transducers and applications in ultrasonic nondestructive testing of waveguides. Ultrasonics 2015;62:3–19.
[29] Thompson RB. A model for the electromagnetic generation of ultrasonic guided waves in ferromagnetic metal polycrystals. IEEE Trans Sonics Ultrason 1978;25(1):7–15.
[30] Ribichini R, Nagy P, Ogi H. The impact of magnetostriction on the transduction of normal bias field emats. NDT & E Int 2012;51:8–15.
[31] Dixon S. The analysis of aerospace adhesively bonded aluminium plates using electromagnetic acoustic transducers (emats), Ph.D. thesis. University of Warwick; 1994.
[32] Ribichini R. Modelling of electromagnetic acoustic transducers, Ph.D. thesis. London: Imperial College; 2011.
[33] Date E, Atkins M, Beaton G. Measurement of the elasticity and ultrasound velocities of steel. Ultrasonics 1971;9(4):209–14.
[34] Papadakis EP, Lynnworth LC, Fowler KA, Carnevale EH. Ultrasonic attenuation and velocity in hot specimens by the momentary contact method with pressure coupling, and some results on steel to 1200 c. J Acoust Soc Am 1972;52(3B):850–7.
[35] Huang S, Zhao W, Zhang Y, Wang S. Study on the lift-off effect of emat. Sens Actuators A: Phys 2009;153(2):218–21.
[36] Dixon S, Fletcher M, Rowlands G. The accuracy of acoustic birefringence shear wave measurements in sheet metal. J Appl Phys 2008;104(11):114901.